THE JOURNAL OF PHYSICAL CHEMISTRY C
A JOURNAL OF THE AMERICAN CHEMICAL SOCIETY

pubs.acs.org/JPCC

Article

Understanding the Effect of Nanoparticle Size on Thermal Conductivity in Amorphous Nanoporous Materials Made from Colloidal Building Blocks

Published as part of The Journal of Physical Chemistry virtual special issue "Horst Weller Festschrift".

Vivian Wall,[▽] Sophia C. King,[▽] Glareh Natalie Kashanchi, Suixuan Li, Man Li, Tiphaine Galy, Darrell I. Harry, Susan E. Ju, Michal Marszewski, Laurent Pilon, Yongjie Hu, and Sarah H. Tolbert*

Cite This: *J. Phys. Chem. C* 2022, 126, 18029−18035

Read Online

ACCESS | Metrics & More | Article Recommendations | Supporting Information

ABSTRACT: In this work, we examined the effect of nanoparticle size on the thermal conductivity of mesoporous silica materials made from colloidal precursors. Porous thin films were synthesized using a polymer-templating method, employing commercial colloidal silica solutions containing nanoparticles 6, 9, and 22 nm in diameter as the silica source and poly(methyl methacrylate) colloids as the template. The ratio of polymer to silica was then varied to produce films with a range of porosities. The thermal conductivity of the films was measured using time domain thermal reflectance, and the results indicated that, for the particle sizes studied, there was a weak dependence of thermal conductivity on particle size. This weak dependence was associated with increased interfacial scattering of heat carriers at the boundaries of the smaller nanoparticles. This work adds to our understanding of the effect of nanostructuring on heat transport in amorphous material systems and improves our ability to design low thermal conductivity materials.

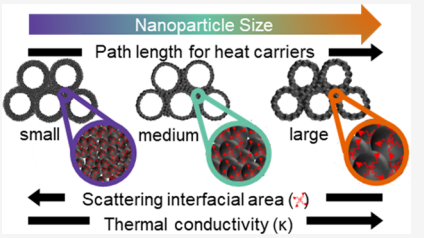

INTRODUCTION

The study of thermal transport is integral to the development of new materials for microelectronics and energy conservation.[1−6] One class of materials of interest is thermally insulating materials, which inspire the exploration of strategies for lowering thermal conductivity.[1,4,5,7] Nanostructuring is known to be an effective method of reducing thermal conductivity due to the variety of structural parameters that can be tuned on the nanoscale, including grain boundary density and nanoporosity.[1,8] In particular, amorphous silica networks with nanoscale pores are of great interest because of their demonstrated ability to reach very low thermal conductivity at high porosity.[1,9−12] Higher porosity reduces the effective density, which decreases the material available for conduction, thereby limiting heat carrier transport. Pores also decrease thermal conductivity by increasing the internal surface area that is available to scatter heat carriers.[13−17] However, the very low density of such materials at high porosity often makes them fragile and hazy or opaque, which limits their use in applications that require durability or optical clarity, such as thermally insulating window coatings. As a result, identifying other nanoscale structural parameters that could decrease thermal conductivity would open up new avenues in the design of thermally insulating materials.

In crystalline materials, particle size has been harnessed as an effective strategy to tune thermal conductivity. Heat carriers propagate in these materials in the form of lattice vibrations called phonons.[5,18] On scales smaller than the phonon mean free path, phonon transport, and therefore thermal conductivity, has been shown to decrease with decreasing feature size.[5,7,16−20] In amorphous materials, however, the influence of feature size on the thermal conductivity is less well understood.[21] Heat transfer in amorphous materials is carried out via many vibrational modes, including propagons, which behave like phonons but with much shorter mean free paths due to the lack of structural order in amorphous networks.[15,16,22] Thus, prevailing theory suggests that heat transfer in amorphous materials is too localized for any size effects to exist.[18] However, Gao and Jelle recently calculated the intrinsic solid-state thermal conductivity of silica nanoparticles as a function of particle size and found a weak effect of size on the nanoparticle thermal conductivity.[18] In addition, Yan et al. recently examined the effect of pore wall thickness on the thermal conductivity of amorphous mesoporous silica thin films made from sol—gel precursors as well as from commercial nanoparticle precursors.[1] The authors found that,

Received: August 1, 2022
Revised: September 20, 2022
Published: October 12, 2022

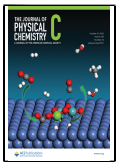

https://doi.org/10.1021/acs.jpcc.2c05444
J. Phys. Chem. C 2022, 126, 18029−18035

for a given porosity, in a continuous sol—gel-based silica network, the thermal conductivity decreased as the thickness of the silica walls decreased. However, no trend in the thermal conductivity with wall thickness was observed for films made from discrete nanoparticle precursors. They attributed this lack of correlation to the fact that the nanoparticles making up the walls were the same size, hypothesizing that there would be an effect of nanoparticle building block size, rather than wall thickness, on thermal conductivity. In this work, we are interested in building upon these studies to experimentally explore the existence of any nanoparticle size effects on the thermal conductivity of amorphous silica nanoparticle-based films.

EXPERIMENTAL METHODS

Materials. The following materials were obtained from commercial suppliers and used without further purification: colloidal suspensions of silica nanoparticles (15 wt %, Nalco 2326, ammonium-stabilized colloidal silica, d = 5 nm, Nalco Chemical Co.; 6−8 wt %, Nyacol LiSol3, lithium-stabilized colloidal silica, d = 2−4 nm, Nyacol Nano Technologies; 40 wt % NexSil 20NH4, ammonium-stabilized colloidal silica, d = 20 nm, Nyacol Nano Technologies); triblock copolymer Pluronic F127 ($EO_{100}PO_{65}EO_{100}$, M_w = 12600 Da, BASF).

Synthesis of Polymer-Templated Mesoporous Silica Films. As purchased, Pluronic F127 or synthesized PMMA colloids (synthesized as described in the Supporting Information) were used as the pore-forming template, and silica colloids of diameters 6, 9, and 22 nm were used to form the randomly agglomerated network. Porous silica films were then made as previously described.[1,23] For the Pluronic F127-templated films, the appropriate mass of Pluronic F127 dissolved in 5 mL of DI H_2O was added to a fixed volume of silica nanoparticles to produce solutions with polymer-to-silica ratios between 0.6 and 1.2 g/g. For the films using PMMA as the template, 5 mL of the PMMA solution was combined with varying volumes of the colloidal silica solutions to produce solutions, again with polymer-to-silica ratios between 0.6 and 1.2 g/g. For each solution, 80 μL was spin-coated onto a plasma-cleaned 1 in. × 1 in. Si substrate. The film thickness was adjusted by controlling the spin speeds. The dried films were aged at 180 °C for 6 h and then calcined in air at 350 °C for 30 min using a 2 °C min^{-1} temperature ramp to remove the polymer.

Full details of the characterization of the calcined films are given in the Supporting Information.

RESULTS AND DISCUSSION

The precursors used in the synthesis of the mesoporous silica thin films and their sizes are depicted in Figure 1. The diameters of the commercial silica colloids were measured from transmission electron microscopy images (TEMs), as seen in Figure 1a,c,e. These measurements yielded diameters of 6 ± 1 nm (Figure 1a), 9 ± 2 nm (Figure 1c), and 22 ± 2 nm (Figure 1e), here called NP6, NP9, and NP22, respectively. All silica nanoparticles were monodisperse, but the particle size distribution broadened as the particle size increased. This can be observed in Figure 1 through the increase in the width of the histograms going from NP6 (Figure 1b) to NP9 (Figure 1d) to NP22 (Figure 1f). The silica colloids were combined with poly(methyl methacrylate) (PMMA) colloids, synthesized according to the previously reported method[1,24] and described

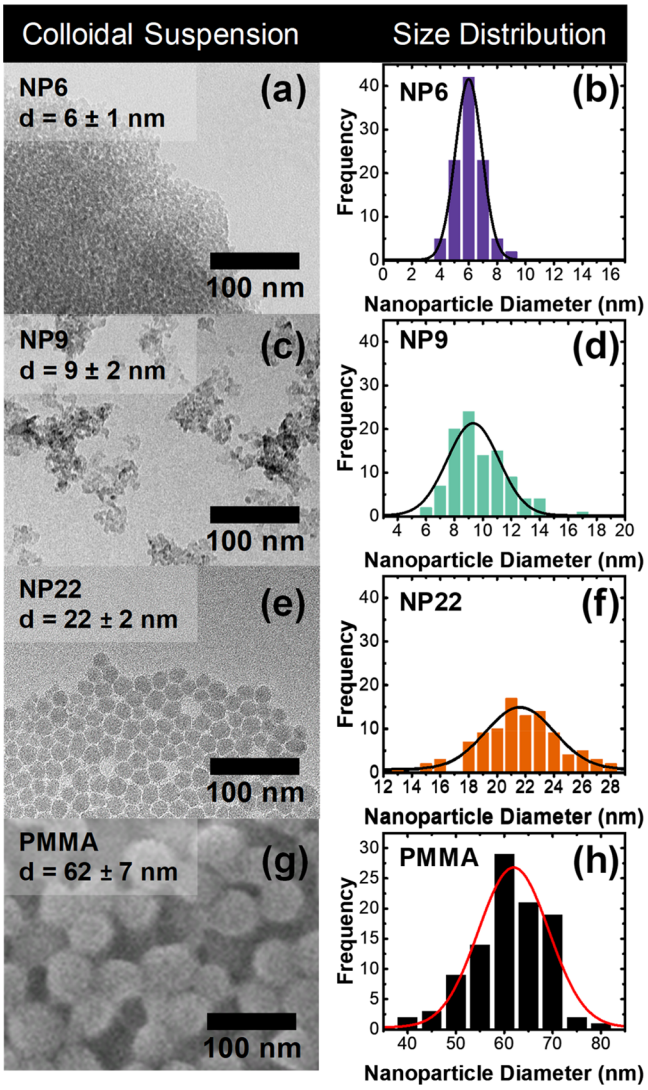

Figure 1. Electron microscope images and size analysis of the commercial silica colloids used as the building blocks for the nanoparticle-based mesoporous silica films. Transmission electron micrographs (TEMs) (a, c, and e) and histograms of nanoparticle diameter distributions (b, d, and f) for commercial silica solutions of diameters 6 ± 1 nm (a and b), 9 ± 2 nm (c and d), and 22 ± 2 nm (e and f). Scanning electron micrograph (SEM) (g) and histogram of the measured diameters (h) of the PMMA colloids used as the polymer template. 100 particles were measured to generate each histogram.

in the Supporting Information, that served as the polymer template. The PMMA colloids had a diameter of 62 ± 7 nm, as depicted in the SEM image (Figure 1g) and the histogram of the measured diameters (Figure 1h).

As purchased, the NP9 and NP22 commercial silica colloids were both stabilized with NH_4^+ counterions, but the NP6 solution was stabilized with Li^+. To ensure that possible differences in thermal conductivity result from differences in nanoparticle size rather than counterion, the Li^+ stabilizing the NP6 solution was exchanged to NH_4^+ using a batch ion-exchange process,[25] as described in the Supporting Information. Figure 2 shows TEM images and size analysis of the Li^+- and NH_4^+-stabilized NP6 solutions and the resulting films. The nanoparticles had approximately the same diameters, as is observed in the TEM images, Figure 2a,d, and the particle size distributions, Figure 2b,e. High-magnification SEM images of

https://doi.org/10.1021/acs.jpcc.2c05444
J. Phys. Chem. C 2022, 126, 18029−18035

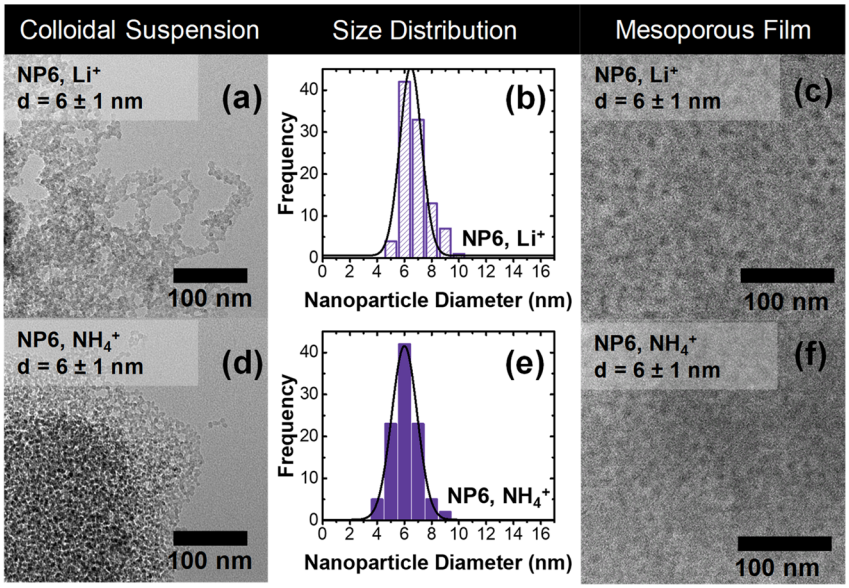

Figure 2. Characterization of the commercial 6 ± 1 nm silica (NP6) particles stabilized with Li^+ (as purchased) and NH_4^+ (ion-exchanged). TEM images depicting the Li^+-stabilized (a) and the ion-exchanged NH_4^+-stabilized (d) 6 nm silica nanoparticles. Histograms used to quantify the measured diameters of the Li^+-stabilized (b) and ion-exchanged NH_4^+-stabilized (e) 6 nm silica nanoparticles, showing that the size distributions were similar. SEM images of films synthesized using Li^+-stabilized (c) and the ion-exchanged NH_4^+-stabilized (f) 6 nm silica nanoparticles with Pluronic F127 as the pore-forming template show that, on the nanoscale, the structure of the films was similar.

the samples, templated with the triblock copolymer Pluronic F127 (Figure 2c,f), show that exchanging the cation did not affect the porous structure of the films. However, examining the thermal conductivity of a small sample set of films made from the Li^+- and NH_4^+-stabilized nanoparticles (Figure 3)

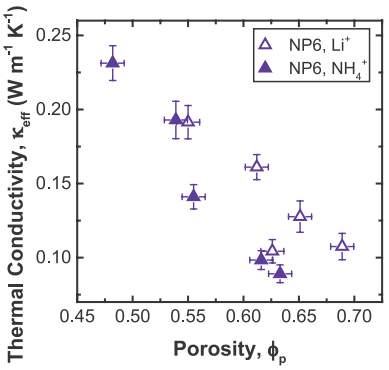

Figure 3. Thermal conductivity as a function of porosity for Li^+-stabilized and ion-exchanged NH_4^+-stabilized 6 nm silica nanoparticles showing that the counterion affects the thermal conductivity of the samples, with ammonium counterions producing lower thermal conductivity materials.

indicated that the films made from the NH_4^+-stabilized colloids had lower thermal conductivity than those made from the Li^+-stabilized colloids. We hypothesize that this difference is due to the fact that the NH_4^+ salt decomposes at the temperatures used for film calcination while the Li^+ salt does not. Thus, Li^+ should remain in the film and may contribute to the thermal conductivity. Therefore, to ensure that the counterion does not affect the measured thermal conductivity of the samples, only NH_4^+-stabilized silica colloids were considered further.

The silica and PMMA colloids were combined in ratios ranging from 0.6 to 1.2 g_{PMMA}/g_{silica} to produce smooth, crack free films with varying porosities. The porous structure of the samples was characterized through SEM, nitrogen porosimetry, and optical interferometry,[26] as shown in Figure 4. Further details of this characterization are provided in the Supporting Information. The SEM images in Figure 4a−f clearly show the porous structure of representative films made from the NP6, NP9, and NP22 silica colloids. The lower magnification images, Figure 4a−c, show that the films produced were smooth and homogeneous with pores well distributed in the network. The pore sizes for all samples were approximately the same, which is expected as the same PMMA template was used to make all films. The higher magnification SEM images, Figure 4d−f, show that the silica colloids that constitute each network were of different sizes and that as the size of the colloids increased, the ability to resolve the individual particles in the network increased as well. This is shown more clearly in Figure S1 in the Supporting Information. Figure S2 further confirms that the networks remain particulate in nature, even down to the smallest colloid sizes used here, even though the colloids cannot be easily resolved with our in-house SEM. Additionally, both Figures 4 and S2 indicate that the colloids are randomly agglomerated in the network and are not organized by the polymer template.

Figure 4g shows the pore size distribution of representative porous powder samples made from each colloid solution at a 1 $g_{PMMA}:g_{silica}$ ratio. The pore size distributions (Figure 4g) establish that each sample had two distinct pore sizes. The first pore size was due to the intrinsic gaps between the nanoparticles. This gap size increased from 5 ± 3 to 8 ± 3 to 11 ± 5 nm as the nanoparticle size increased from 6 to 9 to 22 nm, respectively. A second pore size was observed at approximately 80 nm due to the PMMA-templated pores. This pore size distribution was fairly broad as a result of the polydispersity of the template used. The nitrogen adsorption−desorption isotherms of the samples, shown in the inset of Figure 4g, were complex. According to the IUPAC classification,[27,28] the general shape of the nitrogen adsorption−desorption isotherms at relative pressure less than 0.9

https://doi.org/10.1021/acs.jpcc.2c05444
J. Phys. Chem. C 2022, 126, 18029−18035

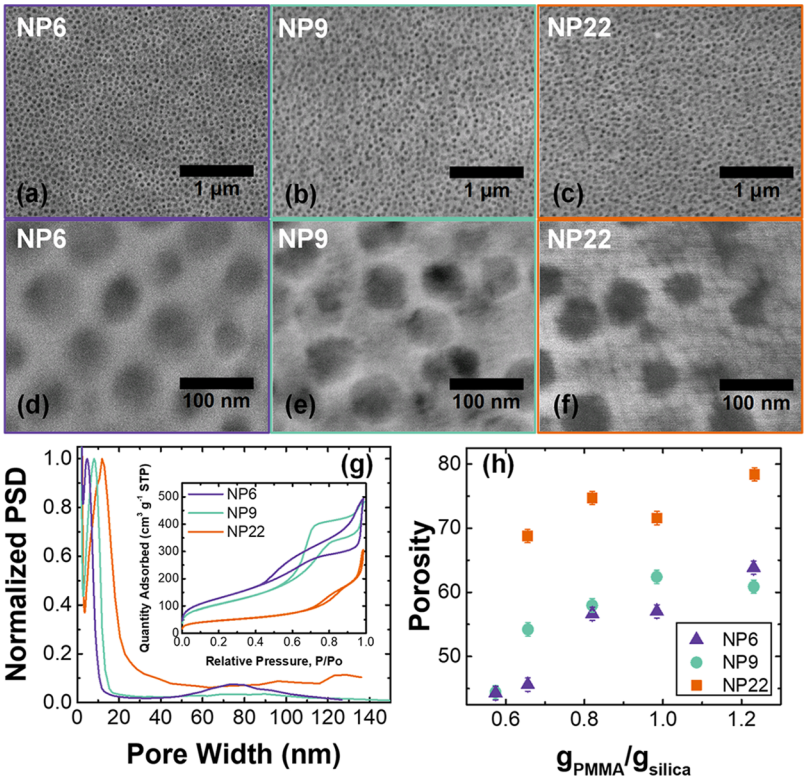

Figure 4. Structural characterization of porous samples made with silica colloids of different sizes, showing the range of porosities used. (a–c) Low-magnification SEMs of PMMA-templated silica films made from commercial colloidal silica solutions with colloid sizes of (a) 6 ± 1, (b) 9 ± 2, and (c) 22 ± 2 nm. These low-magnification images show that the pores were well distributed in the silica network. (d–f) High-magnification SEMs of PMMA-templated silica films made from commercial colloidal silica solutions with colloid sizes of (d) 6 ± 1, (e) 9 ± 2, and (f) 22 ± 2 nm. The individual nanoparticles can be observed as the diameter of the nanoparticles increased. (g) Normalized number-weighted pore size distributions (PSDs) with the inset showing the nitrogen adsorption/desorption isotherms measured at 77 K on powdered samples made from PMMA and commercial silica solutions of different diameters at 1 g_{PMMA}/g_{silica}. The pore widths between 0 and 20 nm were from intrinsic gaps between the particles while those above 50 nm were due to the polymer templating. (h) Porosities of PMMA-templated films used in this study obtained from optical interferometry.

resembled that of a Type IV (a) isotherm with an H2(b) hysteresis loop. Such isotherms are typical of mesoporous materials with fairly narrow pore size distributions and pores connected by narrow necks.[27] This hysteresis was due to the intrinsic gaps between the nanoparticles. Above a relative pressure of 0.9, the volume of nitrogen absorbed did not plateau as is typical of mesoporous samples. Instead, there was another increase in the volume adsorbed that is typical of macroporous samples, resulting from the large pores created by the PMMA template. As the nanoparticle size increased, the relative pressure increased where the volume of adsorbed nitrogen increased, resulting in the observed trend of increasing pore size.

Since the pores created by the PMMA colloids were just outside the range that can be accurately determined by nitrogen porosimetry, the total porosity measured using nitrogen porosimetry was not necessarily an accurate description of the total porosity of the films. As a result, we used an interferometry-based technique to retrieve the total porosity of the films used for the thermal conductivity measurements. The details of this interferometry technique have been previously described.[26] The retrieved porosities depicted in Figure 4h show that, in general, the porosity of the films increased as the ratio of PMMA/silica increased. The samples made from the NP6 and NP9 colloids had similar porosities, while those made from the NP22 colloids had significantly greater porosities. This increased porosity for the larger colloids may be due to larger gaps between colloids in these samples.

Conduction is the primary mode of heat transfer in these mesoporous thin films. Since the porosity of our samples is relatively small and silica absorbs strongly in the infrared part of the spectrum, the contribution of radiation to the overall heat transfer should be negligible. Additionally, the small pore size means that convection is not important to heat transfer in this material.[29] The effective thermal conductivity of the PMMA-templated films as a function of porosity is plotted in Figure 5. The dominant trend in the thermal conductivity across all samples is a decrease in thermal conductivity as porosity increased, with a subtle increase as the particle size increased. In our previous work,[1] we observed a distinct increase in the porosity-dependent thermal conductivity when the thickness of the walls increased in porous silica films with solid continuous silica walls with thicknesses in the range from ∼2 up to ∼25 nm. This led us to hypothesize that such a distinct difference in porosity-dependent thermal conductivity would also occur if the walls were made of nanoparticles with different diameters. However, only small differences can be observed in the present study, indicating that thermal resistance between particles is not dominating. This weak size dependence is similar to the findings of Zhao et al., who studied amorphous regions in silicon nanowires and found that

https://doi.org/10.1021/acs.jpcc.2c05444
J. Phys. Chem. C 2022, 126, 18029−18035

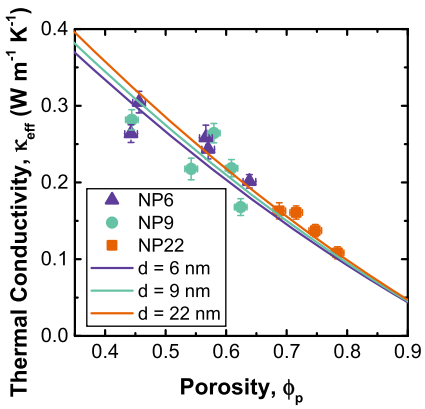

Figure 5. Effective thermal conductivity as a function of porosity for silica nanoparticle-based, PMMA-templated films made from 6 ± 1, 9 ± 2, and 22 ± 2 nm silica nanoparticles, fitted with eq 3. All films were dried under vacuum at 150 °C before the thermal conductivity measurements were conducted to remove any adsorbed water.

thermal conductivity was independent of the length of the amorphous region.[30] We believe that these nearly size-invariant data result from the fact that, even at 6 nm, the sizes of all nanoparticles are still significantly larger than the mean free path length of heat carriers in amorphous silica (ca. 1 nm).[31]

To try to capture the effect of nanoparticle size on the thermal conductivity of the films, we examined the phenomenological model postulated by Liang and Li[32] to predict the thermal conductivity of individual semiconductor nanowires and nanoparticles, as well as dense thin films. Gao and Jelle[18] showed that this model gives good predictions for amorphous silica nanoparticles. The model is given by

$$\frac{\kappa_{\text{eff}}}{\kappa_{\text{SiO}_2}} = p\,\exp\left(-\frac{\lambda}{d}\right)\left[\exp\left(\frac{1-\alpha}{d/L_0 - 1}\right)\right]^{3/2} \quad (1)$$

where κ_{eff} is the effective thermal conductivity of the nanomaterial (in our case, the silica nanoparticles) and p describes the roughness of the surface and can vary from 0 to 1, with 1 representing a smooth surface with a high probability of specular scattering and 0 a very rough surface with a high probability of diffuse scattering. Note that the parameter p for wet chemically synthesized nanoparticles was reported as approximately 0.4.[18,33] Here, λ is the phonon mean free path of silica at room temperature, d is the nanoparticle diameter, and $\alpha = 1 + 2S_V/3R$ is a material constant that depends on the universal gas constant, R = 8.31451 J mol^{-1} K^{-1}, and on the bulk vibrational entropy ($S_V = (H_m/T_m) - R$), where H_m= 9580 J mol^{-1} and T_m = 1986 K are the melting enthalpy and the melting temperature, respectively, for fused silica.[34] Finally, L_0 is a critical size at which all atoms are located at the surface of the nanomaterial and is given by $L_0 = 2(3 - \beta)w$, where β is a dimension parameter (β = 0 for nanoparticles) and w is the interatomic distance (w = 0.16 nm for Si−O bonds).[35]

The effective thermal conductivity of each mesoporous thin film with porosity ϕ_p was then predicted using the Russell model,[36] which has been used for predicting the thermal conductivity of bulk materials with spherical pores and is given by

$$\kappa_{\text{eff}} = \kappa_{\text{SiO}_2}\frac{(1-\phi_p^{2/3})}{(1-\phi_p^{2/3}+\phi_p)} \quad (2)$$

The particle thermal conductivity was then predicted by eqs 1 and 2 so that

$$\frac{\kappa_{\text{eff}}}{\kappa_{\text{SiO}_2}} = \frac{(1-\phi_p^{2/3})}{(1-\phi_p^{2/3}+\phi_p)}p\,\exp\left(-\frac{\lambda}{d}\right)\left[\exp\left(\frac{1-\alpha}{d/d_0 - 1}\right)\right]^{3/2} \quad (3)$$

Applying eq 3 to the films made with the different nanoparticle sizes yields the predictions shown in Figure 5 for each particle diameter. Through least-squares fitting, the data were best described using a mean free path λ = 0.42 nm and a particle roughness p = 0.44. These fits are shown in Figure 5.

We can compare the phonon mean free path λ described by eq 3 to the value determined from the kinetic theory. The kinetic theory relates the thermal conductivity of bulk silica κ_{SiO_2} to the phonon mean free path λ such that $\kappa_{SiO_2} = \frac{1}{3}\rho_{SiO_2}c_{v,SiO_2}v\lambda$.[31] Here, ρ_{SiO_2} is the density of silica (=2210 kg m^{-3}),[37] c_{v,SiO_2} is our previously measured specific heat capacity at constant volume (=750 J kg^{-1} K^{-1}),[1,38] and v is the average sound velocity in the material, obtained from the longitudinal v_l and transversal v_t wave vectors given by $v = \frac{1}{3}v_l + \frac{2}{3}v_t$, with v_l = 5968 m s^{-1} and v_t = 3764 m s^{-1}.[37] From this kinetic model, a phonon mean free path of λ = 0.56 nm in bulk silica (κ_{SiO_2} = 1.4 W m^{-1} K^{-1}) was retrieved, which agrees reasonably well with the value of λ = 0.42 nm that was obtained from eq 3. We also note that the values of λ = 0.42 nm and p = 0.44 are similar to those calculated by Gao and Jelle[18] for individual amorphous silica nanoparticles, namely, λ = 0.59 nm and p = 0.4.

The mean free path λ retrieved was significantly smaller than the size of the nanoparticles. As such, we believe that the marginal decrease in the thermal conductivity observed when the nanoparticle size decreased was not due to heat carrier confinement. Rather, as the diameters of the particles became smaller, the number of particles that make up the wall increased, as did the number of interfaces that were responsible for scattering heat carriers. Therefore, the decrease in thermal conductivity may have been due to an increase in interfacial heat carrier scattering, which may also have been partly responsible for the size-dependent thermal conductivity previously observed in pore walls.[1] To achieve heat carrier confinement, particles smaller than the vibration mean free path of ∼0.5 nm would need to be fabricated. Although small silica fragments can be synthesized, they are very reactive and would likely form a continuous sol−gel network rather than a colloidal network. As such, these results indicate that the best way to further reduce thermal conductivity in amorphous porous materials is by maximizing the interfaces for scattering heat carriers. This can be done through the use of smaller particles, thin walls, or novel materials such as hollow shells or core−shell nanoparticles. Thus, because extremely small colloidal structures cannot be produced, size effects alone appear not to be a good method of further lowering thermal conductivity beyond the standard porosity effects in nanoporous materials built from amorphous building blocks.

CONCLUSION

This study investigated the effect of nanoparticle size on the thermal conductivity of amorphous silica films. We found a weak dependence of thermal conductivity on the diameter of silica nanoparticles, which we attribute to an increase in

https://doi.org/10.1021/acs.jpcc.2c05444
J. Phys. Chem. C 2022, 126, 18029−18035

interfacial scattering of heat carriers. The mean free path for heat carriers extracted from the measured thermal conductivity as a function of porosity across a range of silica colloid sizes was in reasonable agreement with previous measurements for bulk amorphous silica. As such, these results indicate that size effects are not an effective way to lower thermal conductivity in amorphous silica materials unless an unrealistically small size can be reached. This conclusion should be general to any nanoscale amorphous system where the domain size is significantly longer than the vibration mean free path length. The better way to design low thermal conductivity materials is to maximize the interfacial surface area. This study thus adds to our growing understanding of the effect of structure on heat transport in amorphous, nanoporous systems.

■ ASSOCIATED CONTENT

Supporting Information

The Supporting Information is available free of charge at https://pubs.acs.org/doi/10.1021/acs.jpcc.2c05444.

Details of synthesis, structural characterization, and thermal conductivity measurements (PDF)

■ AUTHOR INFORMATION

Corresponding Author

Sarah H. Tolbert − *Department of Chemistry and Biochemistry, University of California, Los Angeles, Los Angeles, California 90095-1569, United States; California NanoSystems Institute, University of California, Los Angeles, Los Angeles, California 90095-8352, United States; Department of Materials Science and Engineering, University of California, Los Angeles, Los Angeles, California 90095-1595, United States;* orcid.org/0000-0001-9969-1582; Phone: (310) 206-4767; Email: tolbert@chem.ucla.edu

Authors

Vivian Wall − *Department of Chemistry and Biochemistry, University of California, Los Angeles, Los Angeles, California 90095-1569, United States;* orcid.org/0000-0002-5354-2415

Sophia C. King − *Department of Chemistry and Biochemistry, University of California, Los Angeles, Los Angeles, California 90095-1569, United States*

Glareh Natalie Kashanchi − *Department of Chemistry and Biochemistry, University of California, Los Angeles, Los Angeles, California 90095-1569, United States*

Suixuan Li − *Department of Mechanical and Aerospace Engineering, University of California, Los Angeles, Los Angeles, California 90095-1597, United States*

Man Li − *Department of Mechanical and Aerospace Engineering, University of California, Los Angeles, Los Angeles, California 90095-1597, United States*

Tiphaine Galy − *Department of Mechanical and Aerospace Engineering, University of California, Los Angeles, Los Angeles, California 90095-1597, United States*

Darrell I. Harry − *Department of Chemistry and Biochemistry, University of California, Los Angeles, Los Angeles, California 90095-1569, United States; Department of Chemistry, Southern University and A&M College, Baton Rouge, Louisiana 70813, United States*

Susan E. Ju − *Department of Chemistry and Biochemistry, University of California, Los Angeles, Los Angeles, California 90095-1569, United States*

Michal Marszewski − *Department of Mechanical and Aerospace Engineering, University of California, Los Angeles, Los Angeles, California 90095-1597, United States;* Present Address: Department of Chemistry and Biochemistry, University of Toledo, Toledo, OH 43606, USA; orcid.org/0000-0002-4157-3046

Laurent Pilon − *Department of Mechanical and Aerospace Engineering, University of California, Los Angeles, Los Angeles, California 90095-1597, United States; Institute of the Environment and Sustainability, University of California, Los Angeles, Los Angeles, California 90095-1496, United States; California NanoSystems Institute, University of California, Los Angeles, Los Angeles, California 90095-8352, United States;* orcid.org/0000-0001-9459-8207

Yongjie Hu − *Department of Mechanical and Aerospace Engineering, University of California, Los Angeles, Los Angeles, California 90095-1597, United States*

Complete contact information is available at: https://pubs.acs.org/10.1021/acs.jpcc.2c05444

Author Contributions

[▽]V.W. and S.C.K. contributed equally to this work.

Notes

The authors declare no competing financial interest.

■ ACKNOWLEDGMENTS

We acknowledge funding support from the U.S. Department of Energy (DOE), Advanced Research Projects Agency-Energy (ARPA-E) under Award No. DE-AR0000738. S.C.K, G.N.K., and T.G are fellows of the NRT-INFEWS: Integrated Urban Solutions for Food, Energy, and Water Management program (Grant No. DGE-1735325). D.I.H. was supported by the UCLA Chemistry, Biochemistry, and Geoscience HBCU Summer Research Program. We acknowledge the use of instruments at the Electron Imaging Center for NanoMachines supported by NIH (1S10RR23057) and the California NanoSystems Institute (CNSI) at UCLA.

■ REFERENCES

(1) Yan, Y.; Li, M.; King, S.; Galy, T.; Marszewski, M.; Kang, J. S.; Pilon, L.; Hu, Y.; Tolbert, S. H. Controlling Thermal Conductivity in Mesoporous Silica Films Using Pore Size and Nanoscale Architecture. *J. Phys. Chem. Lett.* **2020**, *11*, 3731−3737.

(2) Pop, E. Energy Dissipation and Transport in Nanoscale Devices. *Nano Res.* **2010**, *3*, 147−169.

(3) Costescu, R. M.; Cahill, D. G.; Fabreguette, F. H.; Sechrist, Z. A.; George, S. M. Ultra-Low Thermal Conductivity in W/Al_2O_3 Nanolaminates. *Science.* **2004**, *303*, 989−990.

(4) Hrubesh, L. W.; Pekala, R. W. Thermal Properties of Organic and Inorganic Aerogels. *J. Mater. Res.* **1994**, *9*, 731−738.

(5) Cahill, D. G.; Braun, P. V.; Chen, G.; Clarke, D. R.; Fan, S.; Goodson, K. E.; King, W. P.; Mahan, G. D.; Majumdar, A.; Maris, H. J.; et al. Nanoscale Thermal Transport. II. 2003−2012. *Appl. Phys. Rev.* **2014**, *1*, 011305.

(6) Cui, Y.; Li, M.; Hu, Y. Emerging Interface Materials for Electronics Thermal Management: Experiments, Modeling, and New Opportunities. *J. Mater. Chem. C* **2020**, *8*, 10568−10586.

(7) Zhang, H.; Minnich, A. J. The Best Nanoparticle Size Distribution for Minimum Thermal Conductivity. *Sci. Rep.* **2015**, *5*, 8995.

(8) Cahill, D. G.; Ford, W. K.; Goodson, K. E.; Mahan, G. D.; Majumdar, A.; Maris, H. J.; Merlin, R.; Phillpot, S. R. Nanoscale Thermal Transport. *J. Appl. Phys.* **2003**, *93*, 793−818.

(9) Hopkins, P. E.; Rakich, P. T.; Olsson, R. H.; El-Kady, I. F.; Phinney, L. M. Origin of Reduction in Phonon Thermal Conductivity of Microporous Solids. *Appl. Phys. Lett.* **2009**, *95*, 161902.
(10) Hopkins, P. E.; Kaehr, B.; Phinney, L. M.; Koehler, T. P.; Grillet, A. M.; Dunphy, D.; Garcia, F.; Brinker, C. J. Measuring the Thermal Conductivity of Porous, Transparent SiO_2 Films with Time Domain Thermoreflectance. *J. Heat Transfer* **2011**, *133*, 061601.
(11) Deng, Z.; Wang, J.; Wu, A.; Shen, J.; Zhou, B. High Strength SiO_2 Aerogel Insulation. *J. Non. Cryst. Solids* **1998**, *225*, 101−104.
(12) Larkin, J. M.; McGaughey, A. J. H. Thermal Conductivity Accumulation in Amorphous Silica and Amorphous Silicon. *Phys. Rev. B* **2014**, *89*, 144303.
(13) Zhou, W.; Cheng, Y.; Chen, K.; Xie, G.; Wang, T.; Zhang, G. Thermal Conductivity of Amorphous Materials. *Adv. Funct. Mater.* **2020**, *30*, 1903829.
(14) Zhang, H.; Hua, C.; Ding, D.; Minnich, A. J. Length Dependent Thermal Conductivity Measurements Yield Phonon Mean Free Path Spectra in Nanostructures. *Sci. Rep.* **2015**, *5*, 9121.
(15) King, S. C.; Li, M.; Galy, T.; Yan, Y.; Kang, J. S.; Basile, V. M.; Li, Y. L.; Marszewski, M.; Pilon, L.; Hu, Y.; et al. Examining the Role of Atomic Scale Heterogeneity on the Thermal Conductivity of Transparent, Thermally Insulating, Mesoporous Silica−titania Thin Films. *J. Phys. Chem. C* **2020**, *124* (50), 27442−27452.
(16) Wingert, M. C.; Zheng, J.; Kwon, S.; Chen, R. Thermal Transport in Amorphous Materials: A Review. *Semicond. Sci. Technol.* **2016**, *31*, 113003.
(17) Hu, Y.; Zeng, L.; Minnich, A. J.; Dresselhaus, M. S.; Chen, G. Spectral Mapping of Thermal Conductivity through Nanoscale Ballistic Transport. *Nat. Nanotechnol.* **2015**, *10*, 701−706.
(18) Gao, T.; Jelle, B. P. Thermal Conductivity of Amorphous Silica Nanoparticles. *J. Nanoparticle Res.* **2019**, *21*, 108.
(19) Marconnet, A. M.; Asheghi, M.; Goodson, K. E. From the Casimir Limit to Phononic Crystals: 20 Years of Phonon Transport Studies Using Silicon-on-Insulator Technology. *J. Heat Transfer* **2013**, *135*, 061601.
(20) Prasher, R. Thermal Interface Materials: Historical Perspective, Status, and Future Directions. *Proc. IEEE* **2006**, *94*, 1571−1586.
(21) Tsui, B.-Y.; Yang, C.-C.; Fang, K.-L. Anisotropic Thermal Conductivity of Nanoporous Silica Film. *IEEE Trans. Electron Devices* **2004**, *51*, 20−27.
(22) Allen, P. B.; Feldman, J. L.; Fabian, J.; Wooten, F. Diffusons, Locons and Propagons: Character of Atomie Yibrations in Amorphous Si. *Philos. Mag. B* **1999**, *79*, 1715−1731.
(23) Dunphy, D. R.; Sheth, P. H.; Garcia, F. L.; Brinker, C. J. Enlarged Pore Size in Mesoporous Silica Films Templated by Pluronic F127: Use of Poloxamer Mixtures and Increased Template/SiO_2 Ratios in Materials Synthesized by Evaporation-Induced Self-Assembly. *Chem. Mater.* **2015**, *27*, 75−84.
(24) Zou, D.; Ma, S.; Guan, R.; Park, M.; Sun, L.; Aklonis, J. J.; Salovey, R. Model Filled Polymers. V. Synthesis of Crosslinked Monodisperse Polymethacrylate Beads. *J. Polym. Sci. Part A Polym. Chem.* **1992**, *30*, 137−144.
(25) Weldes, H. H. Amine and Ammonium Silicate Solutions. *Ind. Eng. Chem. Prod. Res. Dev.* **1970**, *9*, 249−253.
(26) Galy, T.; Marszewski, M.; King, S.; Yan, Y.; Tolbert, S. H.; Pilon, L. Comparing Methods for Measuring Thickness, Refractive Index, and Porosity of Mesoporous Thin Films. *Microporous Mesoporous Mater.* **2020**, *291*, 109677.
(27) Thommes, M.; Kaneko, K.; Neimark, A. V.; Olivier, J. P.; Rodriguez-reinoso, F.; Rouquerol, J.; Sing, K. S. W. Physisorption of Gases, with Special Reference to the Evaluation of Surface Area and Pore Size Distribution (IUPAC Technical Report). *Pure Appl. Chem.* **2015**, *87*, 1051−1069.
(28) Gregg, S. J.; Sing, K. S. W.; Salzberg, H. W. Adsorption Surface Area and Porosity. *J. Electrochem. Soc.* **1967**, *114*, 279C.
(29) Ebert, H. P.; Caps, R.; Heinemann, U.; Fricke, J.Aerogels - Open-Pored Nanostructured Insulation Materials. *International Symposium on Molecular and Microscale Heat Transfer*; Tanasawa, I., Nishia, S., Eds; Begell House: New York, 1997; pp 545−555.
(30) Zhao, Y.; Liu, X.; Rath, A.; Wu, J.; Li, B.; Zhou, W. X.; Xie, G.; Zhang, G.; Thong, J. T. L. Probing Thermal Transport across Amorphous Region Embedded in a Single Crystalline Silicon Nanowire. *Sci. Rep.* **2020**, *10*, 821.
(31) Kittel, C. Interpretation of the Thermal Conductivity of Glasses. *Phys. Rev.* **1949**, *75*, 972−974.
(32) Liang, L. H.; Li, B. Size-Dependent Thermal Conductivity of Nanoscale Semiconducting Systems. *Phys. Rev. B* **2006**, *73*, 153303.
(33) Teja, A. S.; Beck, M. P.; Yuan, Y.; Warrier, P. The Limiting Behavior of the Thermal Conductivity of Nanoparticles and Nanofluids. *J. Appl. Phys.* **2010**, *107*, 114319.
(34) Lorenz, P.; Zhao, X.; Ehrhardt, M.; Zagoranskiy, I.; Zimmer, K.; Han, B. Nano- and Micro-structuring of Fused Silica Using Time-Delay Adjustable Double Flash ns-Laser Radiation. *Proc. SPIE* **2018**, *10520*, 105201K.
(35) Brown, I. D.; Shannon, R. D. Empirical Bond-strength−Bond-length Curves for Oxides. *Acta Crystallogr., Sect. A* **1973**, *29*, 266−282.
(36) Russell, H. W. Principles of Heat Flow in Porous Insulators. *J. Am. Ceram. Soc.* **1935**, *18*, 1−5.
(37) Density of various solids. In *CRC Handbook of Chemistry and Physics*, 103rd ed.; Lide, D. R., Ed.; CRC Press: Boca Raton, FL, USA, 2005; pp 15−29.
(38) Yan, Y.; King, S. C.; Li, M.; Galy, T.; Marszewski, M.; Kang, J. S.; Pilon, L.; Hu, Y.; Tolbert, S. H. Exploring the Effect of Porous Structure on Thermal Conductivity in Templated Mesoporous Silica Films. *J. Phys. Chem. C* **2019**, *123*, 21721−21730.

NOTE ADDED AFTER ASAP PUBLICATION

This paper was published ASAP on October 12, 2022, with an error in the text under equation 1. The corrected version was reposted on October 17, 2022.

https://doi.org/10.1021/acs.jpcc.2c05444
J. Phys. Chem. C 2022, 126, 18029−18035